Journal of Porous Media, 2(3), 231–249 (1999)

Nonsimilar Combined Convection Flow over a Vertical Surface Embedded in a Variable Porosity Medium

Ali J. Chamkha and Khalil Khanafer

Department of Mechanical and Industrial Engineering, Kuwait University, Safat, 13060 Kuwait

ABSTRACT

The problem of combined forced-free convection flow over an isothermal vertical surface embedded in a variable porosity, porous medium with heat generation or absorption is formulated. The formulation includes the porous medium inertia and boundary effects, variable porosity, and thermal dispersion. The developed governing equations are transformed into nonsimilarity equations that have the advantage of producing their solution at the leading edge of the surface. These equations are then solved numerically subject to appropriate boundary and matching conditions by an implicit, finite-difference method. Comparisons with previously reported numerical and experimental work on the special case where no porous medium is present are performed and found to be in excellent agreement. A parametric study of the physical parameters involved in the problem such as the particle diameter-based Reynolds number, the Grashof number, the flow-based Reynolds number, and the heat generation or absorption coefficient is conducted. The obtained results are illustrated graphically to show interesting features of the solution. It is found that flow separation exists for the case of opposing flow condition and that the presence of thermal dispersion is essential for this type of problem.

Received January 6, 1998; Accepted April 28, 1998

NOMENCLATURE

b, c	empirical constants used in Eq. (4)
C_p	fluid heat capacity
C_F	local skin-friction coefficient defined by Eq. (13)
d	particle diameter
F	reduced stream function
g	acceleration due to gravity
Gr	Grashof number $[g\beta(T_w - T_\infty)L^3/\nu^2]$
k_e	porous medium effective thermal conductivity defined by Eq. (6)
k_f	fluid thermal conductivity
k_s	particle thermal conductivity
K	porous medium permeability
L	characteristic plate length
Nu_x	local Nusselt number defined by Eq. (13)
Q_o	dimensional heat generation or absorption coefficient
Pr	Prandtl number $(\mu c_p/k_f)$
Re	flow Reynolds number $(\rho U_\infty L/\mu)$
Re_m	Reynolds number based on the particle diameter $(\rho U_\infty d/\mu)$
Re_x	local Reynolds number
T	fluid temperature
T_w	wall temperature
T_∞	free-stream temperature
u, v	x and y components of fluid velocity
U_∞	free-stream velocity
x	vertical or tangential distance
y	normal distance
Z	assisting ($Z = 1$) or opposing ($Z = -1$) flow constant

Greek symbols

β	coefficient of thermal expansion
δ	dimensionless heat generation or absorption coefficient $[Q_o L/(\rho c_p U_\infty)]$
η	transformed normal coordinate
ε	porous medium porosity defined by Eq. (4)
ε_o	free-stream porosity
μ	fluid dynamic viscosity
ν	fluid kinematic viscosity (μ/ρ)
ψ	stream function
ρ	fluid density
θ	dimensionless temperature $[(T - T_\infty)/(T_w - T_\infty)]$
ξ	transformed tangential coordinate

Superscripts

$'$	denotes partial differentiation with respect to η

INTRODUCTION

The flow and heat transfer characteristics in porous media have received considerable attention in recent years owing to numerous possible applications. Examples of these applications include geothermal reservoirs, building thermal insulation, chemical catalytic reactors, packed beds, heat exchangers, filtration, petroleum reservoirs, and others. Most of the early studies on porous media have used the Darcy law which is applicable to slow flow and does not account for the effect of a solid boundary, inertia forces, variable porosity, and thermal dispersion effects. In most practical situations such as drying and metal processing, these missing effects are significant. It has been shown by many investigators such as Benenati and Brosilow (1962), Schertz and Bischoff (1969), Vafai (1984), and Vafai et al. (1985) that, for an impermeable surface embedded in a porous medium, the porosity distribution exhibits a peak value close to the boundary and then decays asymptotically beyond that value. As a result, channels of high velocity flow are created close to the boundary which tends to affect the wall friction and heat transfer characteristics significantly. This phenomenon has been called the channeling effect and has been discussed extensively in the literature (see, e.g., Vafai et al., 1985). The porous medium inertial effects have been proven to be important for fast flows. That is, for situations in which the Reynolds number based on the pore diameter and local velocity is greater than order of unity. In this situation, the traditional Darcy law is inappropriate because the pressure drop across the porous medium is not linear but a quadratic relationship with the velocity. Another limitation of the application of the Darcy law is concerned with the presence of a boundary. In this case, the no-slip condition at the boundary cannot be satisfied. In a pioneering work, Vafai and Tien (1981, 1982) were the first to consider boundary and inertial effects on flow and heat transfer in constant and variable porosity porous media. In studies on

spherical particles packed beds, the secondary flow effect caused by the mixing and recirculation of local fluid particles through tortuous paths formed by the spherical solid particles making up the porous medium is classified as thermal dispersion (see Amiri and Vafai, 1994). Cheng and Vortmeyer (1988) and Hunt and Tien (1988) have reported on and discussed the physical effects of thermal dispersion. In addition, the effects of non-Darcian, nonuniform porosity, and thermal dispersion on vertical plate natural convection in porous media have been analyzed by Hong et al. (1987).

Mixed or combined convection heat transfer processes can be found in connection with heat exchangers, electronic devices, solar collectors, energy storage and heat rejection systems, and many others. The combined convection flow over vertical flat plates without porous media has been considered extensively by many investigators such as Lloyd and Sparrow (1970), Oosthuizen and Hart (1973), Wilks (1973), and Ramachandran et al. (1985). Experimental measurements of mixed convection air flow over a vertical isothermal surface were reported by Kliegel (1959) and later by Hishida et al. (1983) and Ramachandran et al. (1985). The effects of heat generation or absorption become important for some situations such as the ones dealing with chemical reactions and dissociating fluids. References to some studies dealing with these effects can be found in the articles by Sparrow and Cess (1961), Vajravelu and Nayfeh (1992), Chamkha (1996, 1997), and Vajravelu and Hadjinicolaou (1997). All of these references considered temperature-dependent heat generation (source) or absorption (sink).

There has also been considerable interest in investigating combined convection heat transfer from a vertical plate embedded in uniform porous media for different flow and thermal wall conditions by many researchers. Takhar et al. (1990) investigated mixed convection flow over a hot vertical plate in non-Darcian porous media. Hsieh et al. (1993) reported numerical solutions for mixed convection along a vertical flat plate embedded in a uniform porosity medium for the cases of variable wall temperature and variable wall heat flux. Hooper et al. (1994) considered the same problem with surface suction or injection for the case of uniform wall temperature. Other works dealing with combined convection in porous media can be found in the articles by Gill and Minkowycz (1988), Chen and Chen (1990), Shenoy (1992), and Aldoss et al. (1995).

Motivated by all of the above referenced work and the significant possible applications of porous media in many industries, it is of interest in this article to consider non-Darcian combined convection flow over a vertical impermeable surface embedded in a porous medium having a variable porosity distribution in the presence of thermal dispersion and heat generation effects.

GOVERNING EQUATIONS

Consider steady, laminar, combined convection flow along a vertical impermeable semiinfinite surface embedded in a variable porosity porous medium in the presence of heat generation or absorption effects. The plate or surface is coincident with the half plane $y > 0$, $x \geq 0$ and the flow far from the plate is a uniform stream in the x-direction parallel to the plate (see Fig. 1). All physical properties of the fluid are assumed to be constant except the density in the buoyancy term of the momentum, equation. Both the fluid and the porous medium are assumed to be in local thermal equilibrium. The governing equations for this investigation are based on the balance laws of mass, linear momentum, and energy modified to account for the presence of the porous medium Darcian effects and non-Darcian boundary, inertia, and thermal dispersion effects in addition to the buoyancy and heat generation or absorption effects. The boundary-layer form of these equations

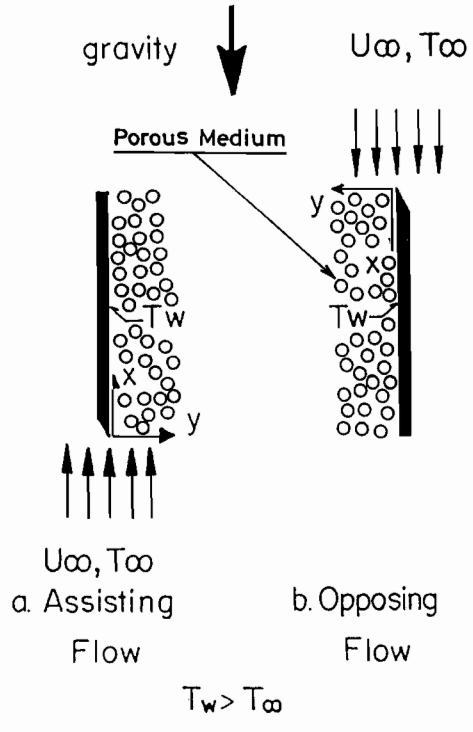

Figure 1. Flow configuration and coordinate system.

(taking into account the Boussinesq approximation) can be written as

$$\frac{\partial u}{\partial x}+\frac{\partial v}{\partial y}=0 \tag{1}$$

$$\frac{\rho}{\varepsilon^2}\left(u\frac{\partial u}{\partial x}+v\frac{\partial u}{\partial y}\right)=Z\rho g\beta(T-T_\infty)+\frac{\mu}{\varepsilon}\frac{\partial^2 u}{\partial y^2}-\frac{\mu}{K(y)}u-\rho C(y)u^2 \tag{2}$$

$$\rho C_p\left(u\frac{\partial T}{\partial x}+v\frac{\partial T}{\partial y}\right)=\frac{\partial}{\partial y}\left(k_e\frac{\partial T}{\partial y}\right)+Q_o(T-T_\infty) \tag{3}$$

where x and y are the tangential and normal distances, respectively; u, v, and T are the fluid x and y components of velocity and temperature, respectively; ρ, μ, C_p, and Q_o are the fluid density, dynamic viscosity, heat capacity, and heat generation or absorption coefficient, respectively; g, β, and T_∞ are the acceleration due to gravity, coefficient of thermal expansion, and the free-stream temperature, respectively; ε, K, C, and k_e are the porous medium porosity, permeability, inertia coefficient, and effective thermal conductivity, respectively. Z is a constant such that $Z = 1$ corresponds to assisting or aiding flow and $Z = -1$ corresponds to opposing flow.

Equations (1) through (3) are supplemented by constitutive equations for the variations of the porosity, permeability, inertia coefficient, and thermal conductivity of the porous medium. It has been shown by Vafai et al. (1985) that the results obtained experimentally by Benenati and Brosilow (1962) in their study on void fraction distribution in packed beds that give the functional dependence of the porosity on the normal distance from the boundary can be represented by the exponential relationship

$$\varepsilon=\varepsilon_o(1+b\exp(-cy/d)) \tag{4}$$

where ε_o is the free-stream porosity, d is the particle diameter, b and c are empirical constants that depend on the ratio of the bed to particle diameter. The values for ε_o, b, and c were chosen to be 0.38, 1, and 2, respectively. These values were found to give good approximation to the variable porosity data given by Benenati and Brosilow (1962) for a particle diameter $d = 5$ mm. These same values were also employed by Nithiarasu et al. (1997) on their work on natural convection heat transfer in a fluid-saturated variable porosity medium inside a rectangular enclosure. The type of decay of porosity as the normal distance increases given by Eq. (4) is well established and has been used extensively in studies on flow in porous media with variable porosity. It is also established that K and C vary with porosity as follows:

$$K(y)=\frac{d^2\varepsilon^3}{150(1-\varepsilon)^2},\qquad C(y)=\frac{1.75}{\sqrt{150\varepsilon K(y)}} \tag{5a,b}$$

Following Amiri and Vafai (1994), the effective thermal conductivity of the porous medium is given by

$$k_e=k_f\left(\varepsilon+0.1PrRe_m\frac{u}{U_\infty}\right)+(1-\varepsilon)\,k_s \tag{6}$$

where k_f is the clear fluid thermal conductivity, k_s is the thermal conductivity of the porous medium, Pr ($\mu C_p/k_f$) is the Prandtl number, Re_m($=\rho U_\infty d/\mu$) is the Reynolds number based on the particle diameter, and U_∞ is the free-stream velocity. For a typical range of free stream air velocity at standard conditions of $0.3 \le U_\infty \le 3$ m per second, it can be concluded that the range of applicable values of Re_m is between 100 and 900 for a particle diameter of 5 mm. These values of Re_m were used in producing the numerical results to be reported subsequently.

The physics of the problem suggests the following boundary conditions:

$$\begin{aligned}&u(x,0)=0,\qquad v(x,0)=0,\qquad T(x,0)=T_w\\&u(x,y)\to U_\infty,\qquad T(x,y)\to T_\infty \text{ as } y\to\infty\end{aligned} \tag{7}$$

where T_w is the constant surface or wall temperature.

The flow and heat transfer problem represented by Eqs. (1) through (7) has no similar or exact solutions. To facilitate the solution of the problem in the whole regime of mixed or combined convection, it is convenient to employ the following nonsimilarity transformations similar to those used earlier by Ramachandran et al. (1985):

$$\begin{aligned}&\xi=\frac{x}{L},\qquad \eta=\left(\frac{U_\infty}{\nu x}\right)^{1/2}y,\qquad u=\frac{\partial\Psi}{\partial y},\\&v=-\frac{\partial\Psi}{\partial x}\qquad \Psi(x,y)=(\nu U_\infty x)^{1/2}F(\xi,\eta),\\&T(x,y)-T_\infty=(T_w-T_\infty)\theta(\xi,\eta)\end{aligned} \tag{8}$$

where L is a characteristic length of the plate, $\nu(=\mu/\rho)$ is the kinematic viscosity of the fluid, and ψ is the stream function which identically satisfy the continuity equation.

Substituting Eqs. (8) into the governing equations result in the transformed equations:

$$F'''+\frac{FF''}{2\varepsilon}-\frac{\xi\varepsilon}{DaRe}F'-\frac{1.75\xi F'^2}{\sqrt{150\varepsilon^3 Da}}+Z\xi\varepsilon\frac{Gr}{Re^2}\theta=\frac{\xi}{\varepsilon}\left(F'\frac{\partial F'}{\partial\xi}-F''\frac{\partial F}{\partial\xi}\right) \tag{9}$$

$$\frac{r_k}{Pr}\theta'' - \left(\frac{\varepsilon_o bc}{PrRe_m}\sqrt{\xi Re}\exp\left(-\frac{c\sqrt{\xi Re}\,\eta}{Re_m}\right)\right.$$
$$\left. - 0.1\,Re_m F'' - \frac{F}{2}\right)\theta' + \xi\delta\theta = \xi\left(F'\frac{\partial\theta}{\partial\xi} - \theta'\frac{\partial F}{\partial\xi}\right) \tag{10}$$

where a prime denotes partial differentiation with respect to η and

$$\varepsilon = \varepsilon_o\left(1 + b\exp\left(-\frac{c\sqrt{\xi Re}}{Re_m}\eta\right)\right),$$
$$Da = \frac{Re_m^2}{Re^2}\frac{\varepsilon^3}{150(1-\varepsilon)^2}, \qquad \delta = \frac{Q_o L}{\rho C_p U_\infty},$$
$$Re = \frac{U_\infty L}{\nu}, \qquad Gr = \frac{g\beta(T_w - T_\infty)L^3}{\nu^2}, \tag{11}$$
$$r_k = \frac{k_e}{k_f} = \varepsilon + 0.1PrRe_m F'$$

It should be noted here that the porous medium is assumed to be nonmetallic (glass fibers), such that $k_s << k_f$ and, therefore, the last term of Eq. (6) is neglected. The transformed boundary conditions become

$$F'(\xi, 0) = 0; \qquad F(\xi, 0) = 0; \qquad \theta(\xi, 0) = 1$$
$$F'(\xi, \eta) \to 1; \qquad \theta(\xi, \eta) \to 0 \text{ as } \eta \to \infty \tag{12}$$

Important physical quantities for this flow and heat transfer situation are the local skin-friction coefficient and the local Nusselt number. These can be expressed, respectively, in dimensionless form as follows:

$$C_F Re_x^{1/2} = 2F''(\xi, 0); \; Nu_x Re_x^{-1/2} = -\theta'(\xi, 0) \tag{13}$$

where $Re_x = U_\infty x/\nu$ is the local Reynolds number.

NUMERICAL TECHNIQUE

The problem represented by Eqs. (9) through (12) is obviously nonlinear and exhibits no closed-form solution. Therefore, it must be solved numerically. The tridiagonal, implicit, iterative, finite-difference method discussed by Blottner (1970) has proven to be successful for the solution of boundary-layer problems. For this reason, it is adopted in the present work.

All first-order derivatives with respect to ξ are represented by three-point backward difference formulae. All second-order differential equations in η are discretized using three-point central difference quotients while all first-order differential equations in η are discretized using the trapezoidal rule. The computational domain was divided into 41 nodes in the ξ direction and 101 nodes in the η direction. Constant step sizes in both the ξ and η directions such that $\Delta\xi = 0.025$ and $\Delta\eta = 0.01$ are employed. The governing equations are then converted into sets of linear tridiagonal algebraic equations that are solved by the Thomas Algorithm (see Blottner, 1970) at each iteration. The convergence criterion employed in the present problem required that the difference between the current and the previous iterations be 10^{-5}. It should be mentioned that many numerical experimentations were performed by altering the step sizes in both directions to ensure accuracy of the results and to assess grid independence and it was found that a computational domain of (ξ, η) = (41, 101) grid points is adequate to produce accurate results. Many results were obtained throughout the course of this work. A representative set is presented in Figs. 2 through 21 to show the effects of the physical parameters on the solutions. In all of the results to be reported subsequently, Pr was equated to 0.7 corresponding to air.

RESULTS AND DISCUSSION

To assess the accuracy of the numerical method, a comparison between the numerical results obtained in this study and the numerical and experimental solutions reported earlier by Ramachandran et al. (1985) for mixed convection assisting flow of air ($Pr = 0.7$) along a vertical plate in the absence of a porous medium is performed. The results of this comparison are reported in Fig. 2 for the tangential velocity F' and the temperature θ profiles at various values of the modified mixed convection parameter $\xi^* = \xi\, Gr/Re^2$. It should be mentioned here that ξ^* is the same ξ employed by Ramachandran et al. (1985). It is obvious from this figure that excellent agreement between the present results of both F' and θ and those reported by Ramachandran et al. (1985) exists. This favorable comparison lends confidence to the numerical results to be reported subsequently.

Figures 3 and 4 present typical tangential velocity (F') and temperature (θ) profiles at $\xi = 1$ for various values of the Reynolds number based on the particle diameter Re_m with all other parameters being fixed, respectively. Unless otherwise stated, these and all subsequent figures correspond to the aiding or assisting flow condition. It is clearly seen from these figures that both the distributions of F' and θ increase while both the hydrodynamic and thermal boundary-layer thicknesses decrease as Re_m increases. In addition, as Re_m becomes greater than 300, an overshoot above the free stream value in the velocity profile occurs. This overshoot phenomenon occurs close to the boundary

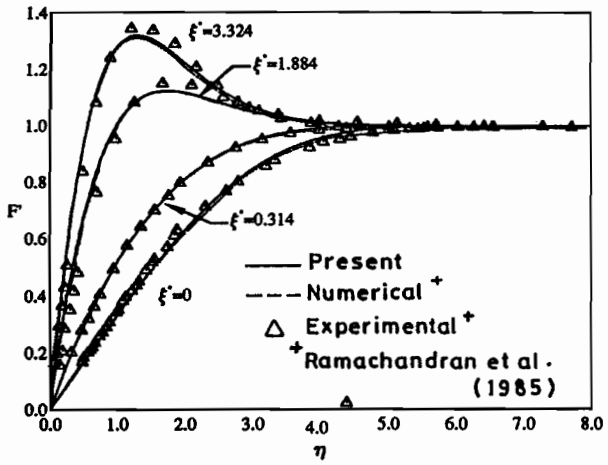

(a)

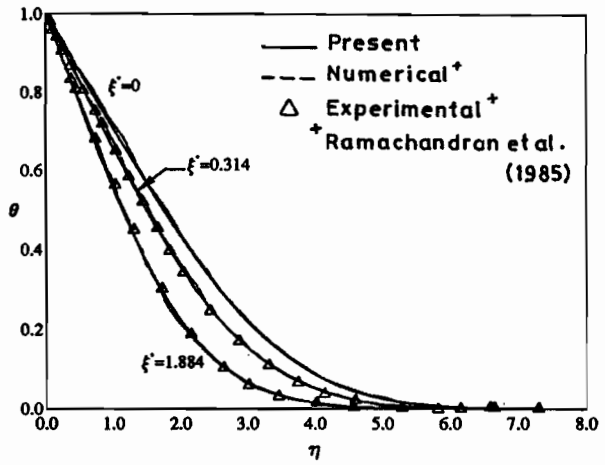

(b)

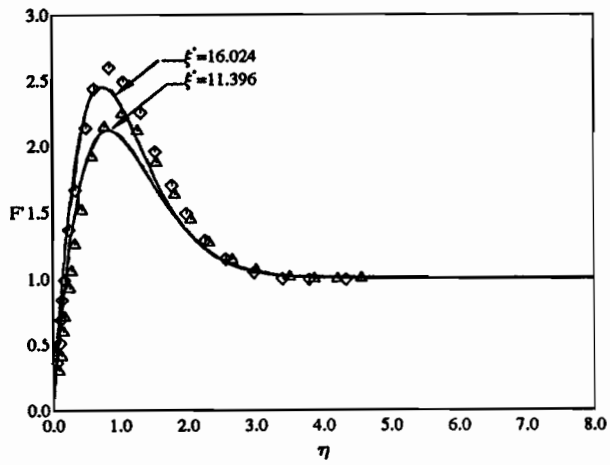

(a)

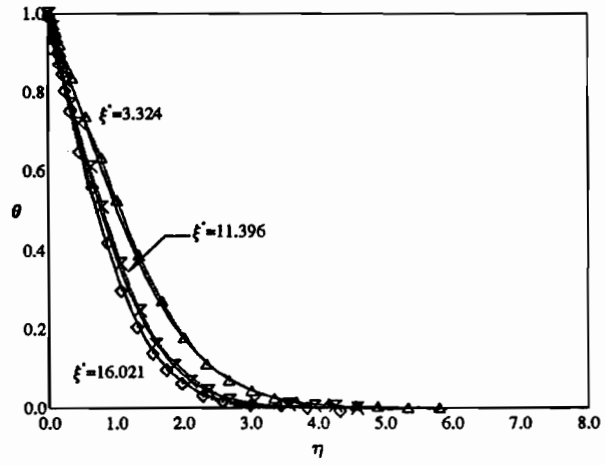

(b)

Figure 2. Comparison of the tangential velocity and temperature profiles between present and Ramachandran et al. (1985) solutions.

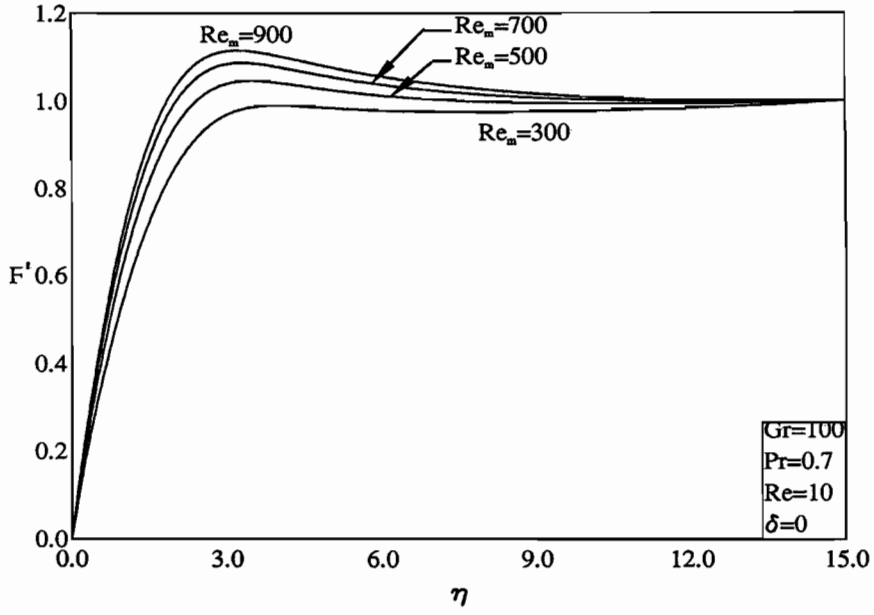

Figure 3. Effect of Re_m on the tangential velocity profiles.

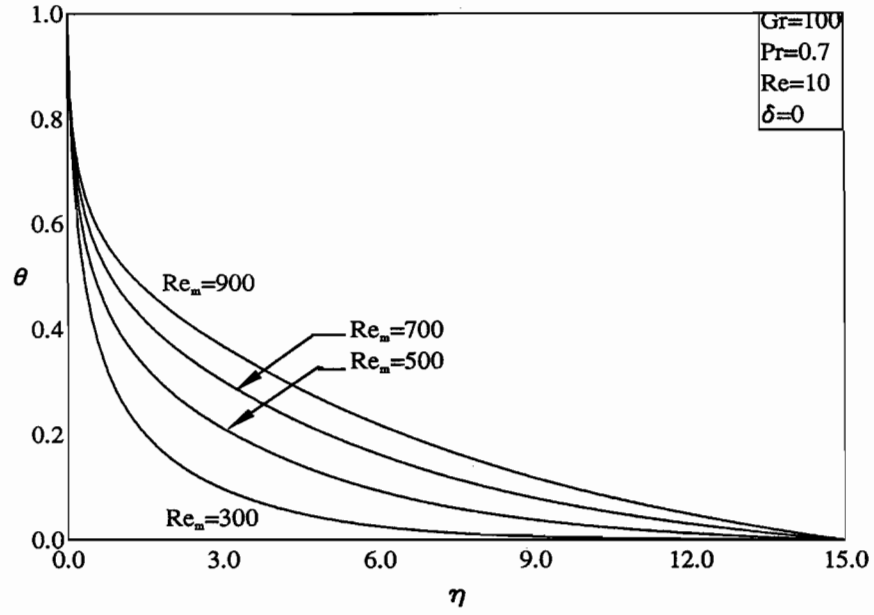

Figure 4. Effect of Re_m on the temperature profiles.

and has been verified experimentally in the work of Ramachandran et al. (1985).

Figures 5 and 6 depict the influence of Re_m on both the local skin-friction coefficient $C_F^*(=C_F Re_x^{1/2})$ and the local Nusselt number $Nu_x^*(=Nu_x Re_x^{1/2})$ along the vertical plate, respectively. Increases in the particle-diameter-based Reynolds number Re_m have the tendency to increase the slopes of both the tangential velocity $F'(\xi, 0)$ and temperature profiles $-\theta'(\xi, 0)$ at the wall. This has the direct effect of increasing both C_F^* and Nu_x^* as is evident from Figs. 5 and 6. In addition, it is observed from Fig. 6 that the Nusselt number curves for $Re_m = 500$, 700, and 900 intersect far from the plate's leading edge and the point of intersection appears to be shifting toward the leading edge of the plate as Re_m is increased further. This behavior is believed to be related to or associated with the thermal dispersion effect. Inspection of Eq. (10) shows that as Re_m is increased, the second term becomes very small while the first and third terms dominate for small ξ. As the flow moves along the plate and ξ increases, some contributions from the last terms multiplying ξ of Eq. (10) that have the opposite sign of the other dominating terms tend to level off or slow down the increases in the values of $Nu_x Re_x^{1/2}$ at the higher ξ locations. This, in turn, causes the curves at the higher Re_m values to intersect.

Figures 7 through 10 illustrate the effects of the Grashof number Gr on the tangential velocity and temperature profiles at $\xi = 1$ and the local skin-friction and Nusselt number distributions along the plate for a fixed flow Reynolds number $Re = 10$, respectively. Increasing the values of Gr (that is, increasing the buoyancy effects) has the tendency to increase the coupling between the flow and thermal distributions. This causes higher velocity and temperature distributions and higher wall gradients. In addition, the overshoot phenomenon mentioned previously becomes more pronounced as the buoyancy effects become high ($Gr > 100$). The increased wall gradients predicted in the velocity and temperature $[-\theta'(\xi, 0)]$ profiles as Gr increases produce higher wall friction coefficients and Nusselt numbers. However, for $Gr = 1000$, that is $Gr/Re^2 = 10$ (high buoyancy effects), the Nusselt number is predicted to be lower than that of $Gr = 500$ around $\xi = 0.3$. These facts are evident from Figs. 7 through 10.

The variations of $F'(1, \eta)$, $\theta(1, \eta)$, $C_F^*(\xi)$, and $Nu_x^*(\xi)$ that are brought about by varying the flow Reynolds number Re for a fixed value of $Gr = 100$ are given in Figs. 11 through 14, respectively. The shown values of $Re = 2$, 3, 5, and 10 for $Gr = 100$ correspond to mixed convection parameter values $Gr/Re^2 = 25$, 11.11, 4, and 1, respectively. That is, lower values of Re correspond to the buoyancy-dominated regime whereas higher values of Re correspond to the forced convection-dominated regime. Therefore, as

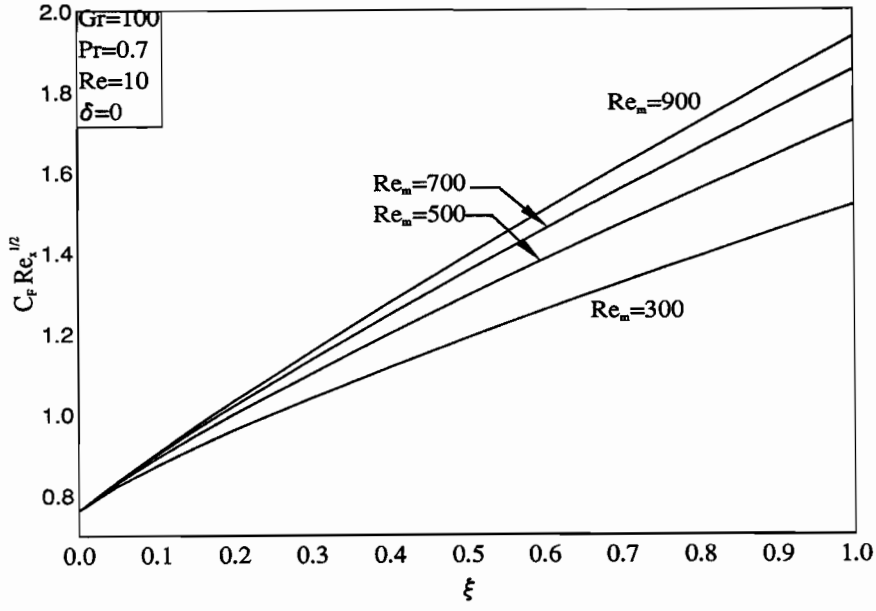

Figure 5. Effect of Re_m on the local skin-friction coefficient.

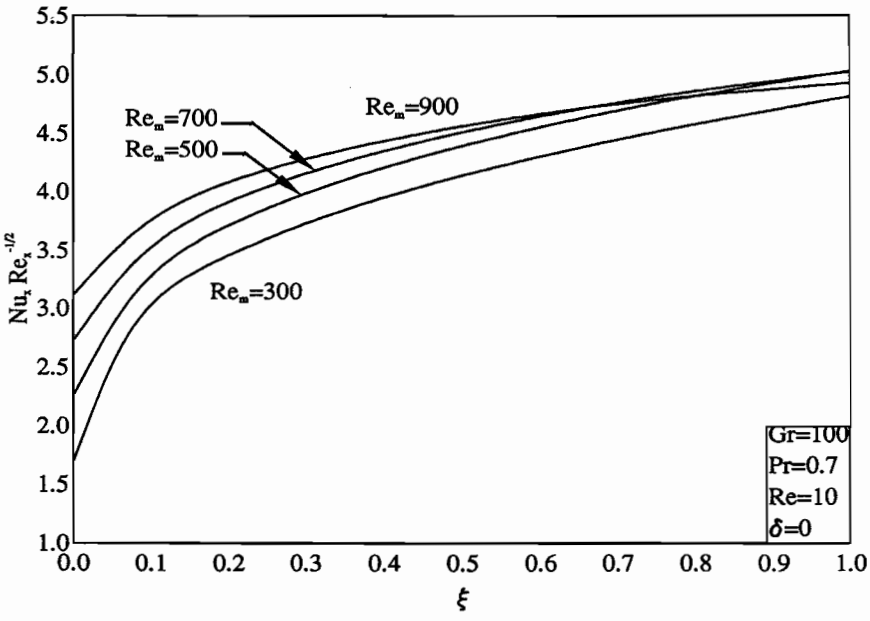

Figure 6. Effect of Re_m on the local Nusselt number.

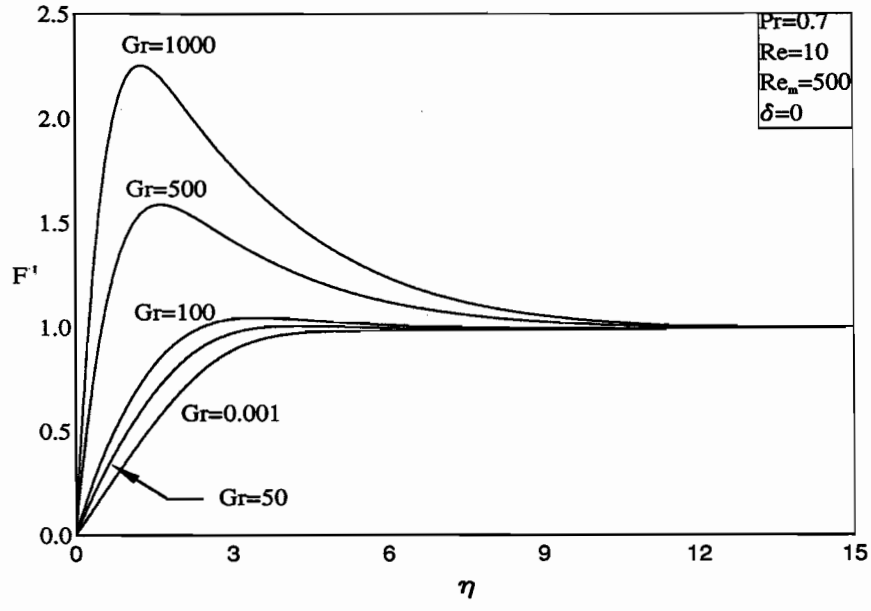

Figure 7. Effect of *Gr* on the tangential velocity profiles.

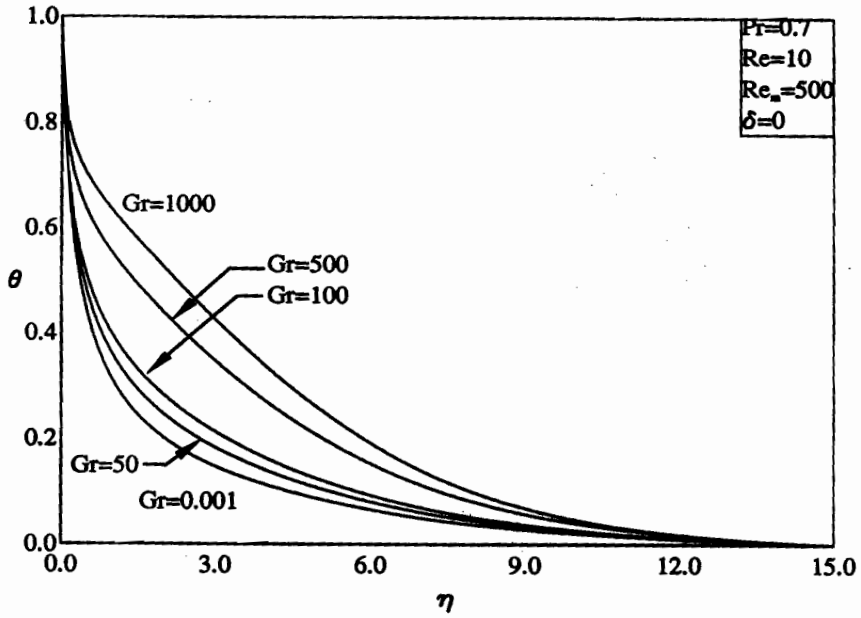

Figure 8. Effect of *Gr* on the temperature profiles.

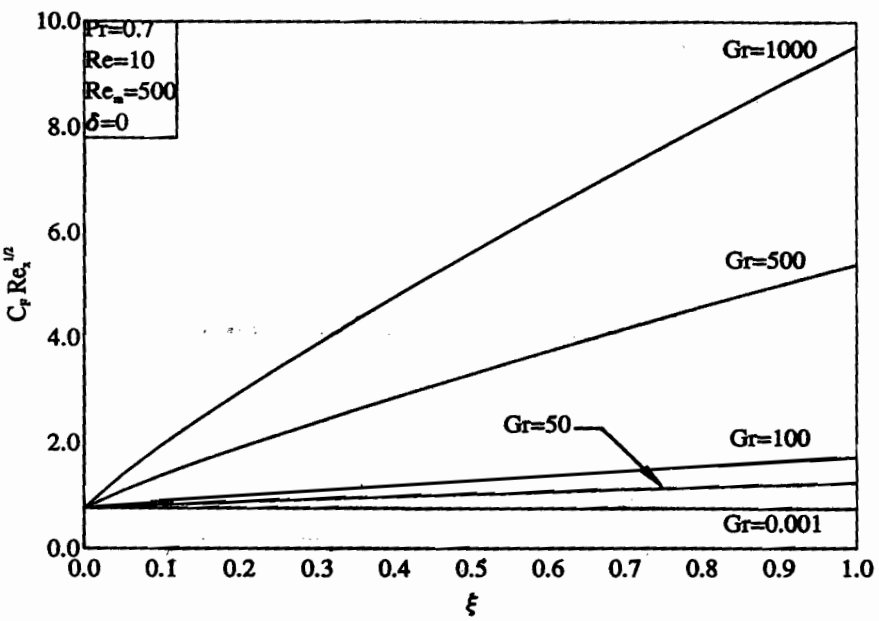

Figure 9. Effect of *Gr* on the local skin-friction coefficient.

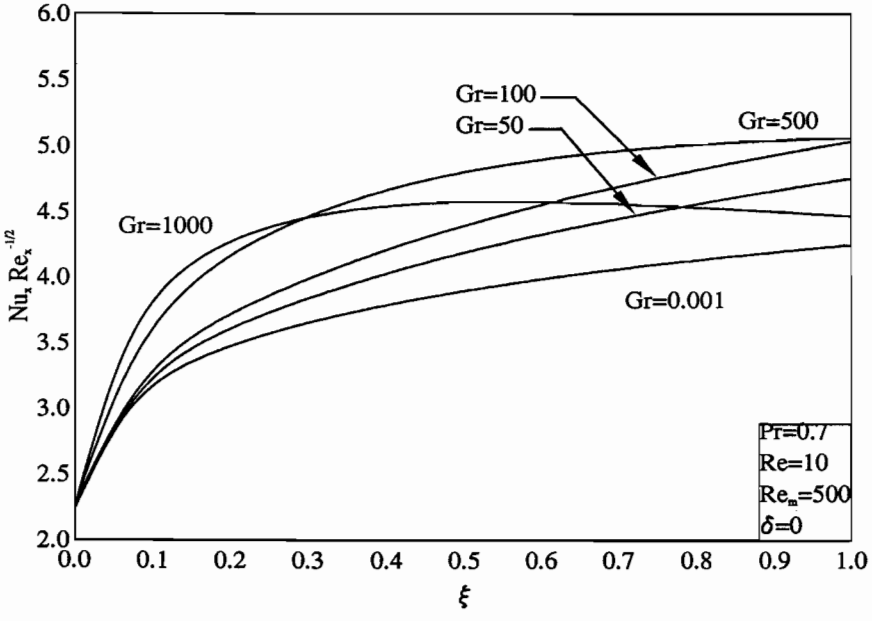

Figure 10. Effect of *Gr* on the local Nusselt number.

expected, increases in *Re* cause decreases in F' and C_F^* values at every location along the plate and increases in θ and Nu_x^* values along the plate. These behaviors are shown clearly in Figs. 11 through 14, respectively. It is also observed that for $Re = 10$ ($Gr/Re^2 = 1$) the skin-friction coefficient is almost constant whereas for small values of *Re* ($Re = 2$) the formation of peaks in the values of Nu_x^* close to the leading edge of the plate is predicted. It is now obvious from Figs. 10 and 14 that the distribution of the Nusselt number Nu_x^* along the plate's tangential distance ξ tends to behave differently for higher values of Gr/Re^2 (free convection-dominated regime) than for lower values (forced convection-dominated regime). In the former regime, Nu_x^* is shown to be decreasing after a certain distance from the leading edge of the plate while in the latter regime Nu_x^* keeps on increasing with ξ. Again, and as discussed for Re_m, this phenomenon is probably due to the presence of the variable porosity and thermal dispersion effects. As the mixed convection parameter Gr/Re^2 increases, the thermal buoyancy-induced flow increases and, therefore, the second term and the term before last in Eq. (10) which have the opposite sign of the other terms increase in magnitude, causing retardation in the wall heat transfer. For small ξ this behavior is minimal. However, it becomes more pronounced for larger values of ξ. As a result of this, the wall heat transfer increasing behavior caused by the conductive and convective terms are overcome by the retarding effect caused by the thermal dispersion effects.

All of the figures discussed in the preceding paragraphs were obtained for a neutral fluid ($\delta = 0$). To illustrate the possibility that the fluid can act as a thermal source (heat generation) or a thermal sink (heat absorption), the heat generation or absorption coefficient δ is allowed to vary separately. Figures 15 through 18 elucidate the features of $F'(1, \eta)$, $\theta(1, \eta)$, $C_F^*(\xi)$, and $Nu_x^*(\xi)$ as δ is altered. It is a known fact that heat generation effects cause the fluid temperature to increase. This has the tendency to increase the thermal buoyancy effects, thus causing higher buoyancy-induced flow velocities. On the other hand, heat absorption produces the opposite effect, namely decreases in the temperature and velocity values along the plate. These behaviors are clear from Figs. 15 and 16. In addition, enhanced skin-friction distributions and reductions in the wall heat flux along the plate are predicted as the values of δ increase. This is due to the increases in the wall slopes of the tangential velocity profiles [$F''(\xi, 0)$] and the decreases in the negative wall slopes of the temperature profiles [$-\theta'(\xi, 0)$] as δ increases. This is evident from Figs. 17 and 18. Furthermore, it is observed that the Nusselt number

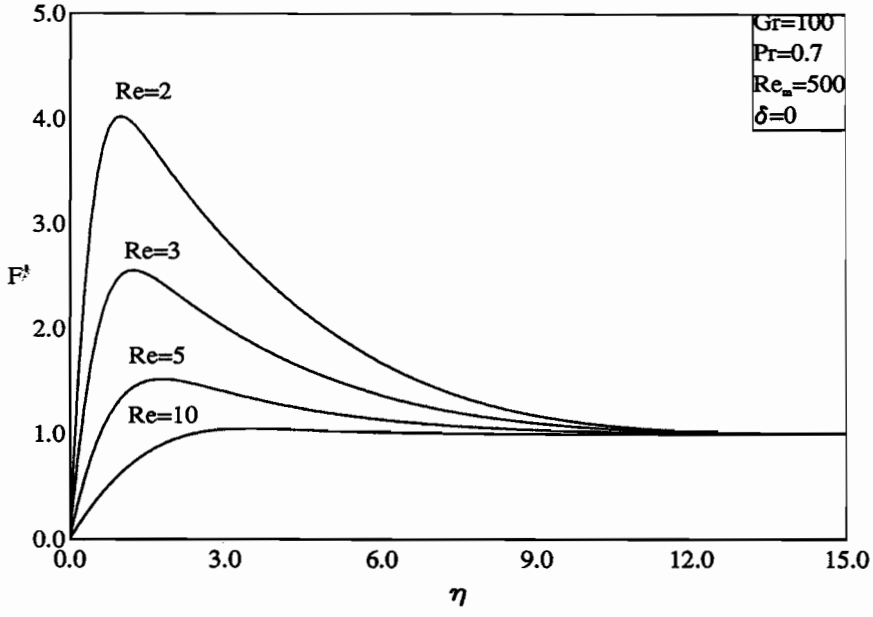

Figure 11. Effect of *Re* on the tangential velocity profiles.

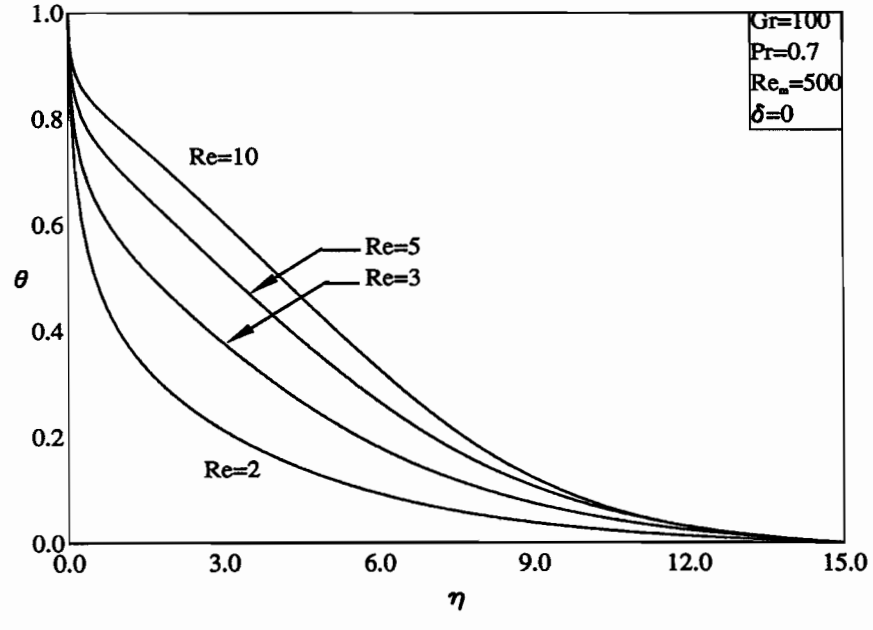

Figure 12. Effect of *Re* on the temperature profiles.

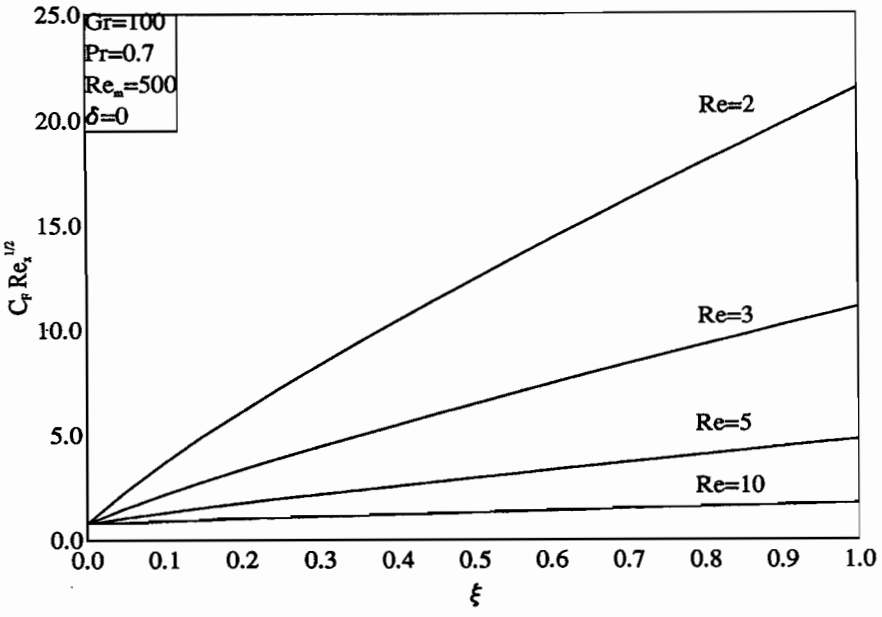

Figure 13. Effect of *Re* on the local skin-friction coefficient.

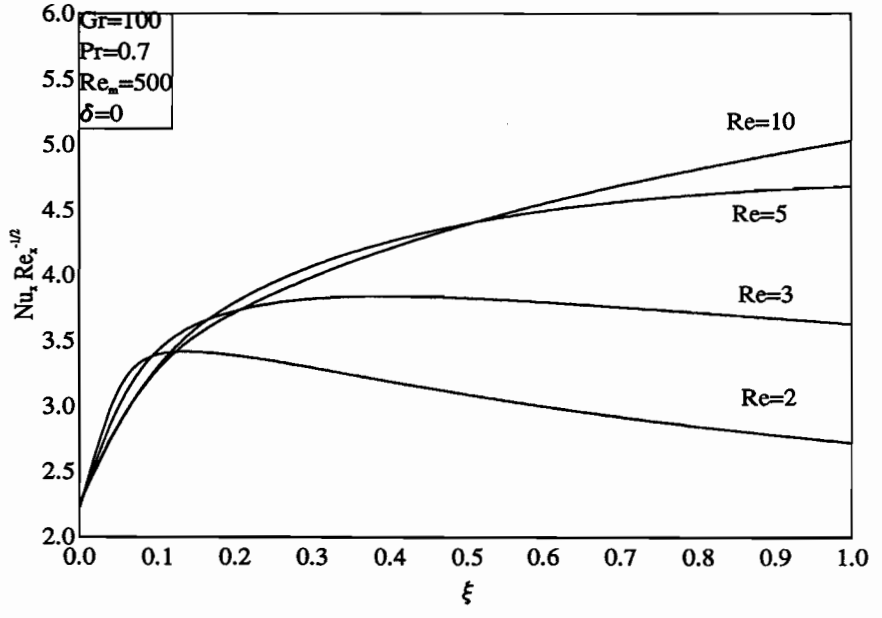

Figure 14. Effect of *Re* on the local Nusselt number.

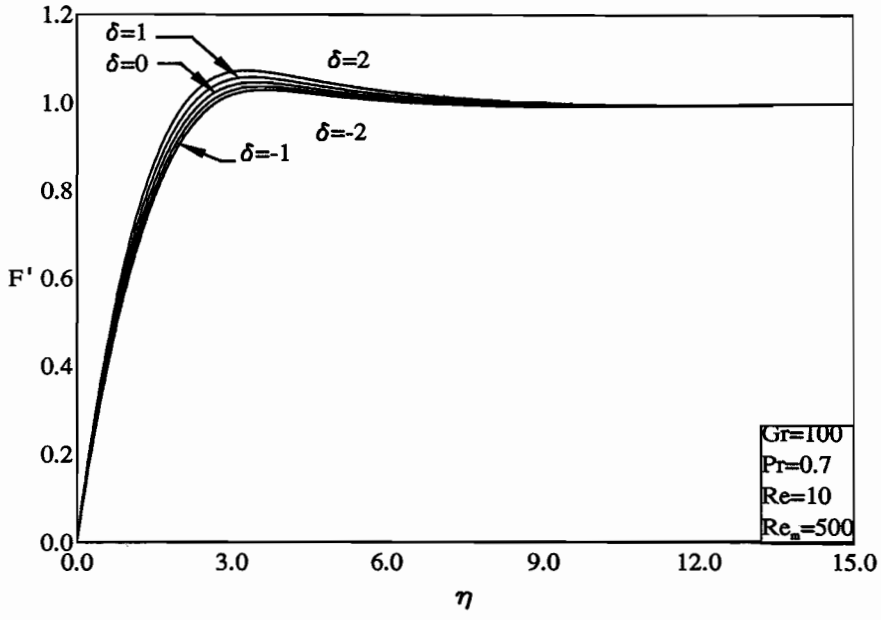

Figure 15. Effect of δ on the tangential velocity profiles.

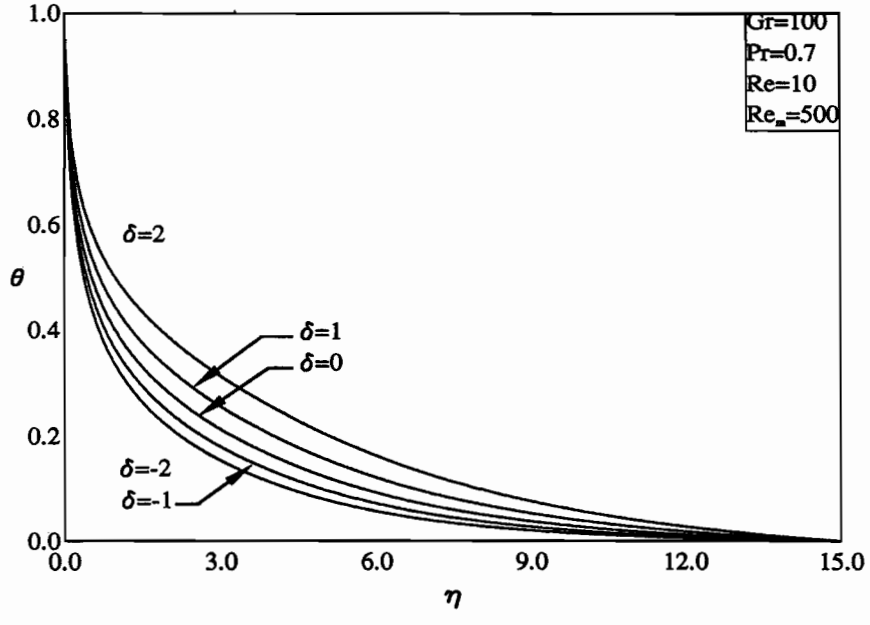

Figure 16. Effect of δ on the temperature profiles.

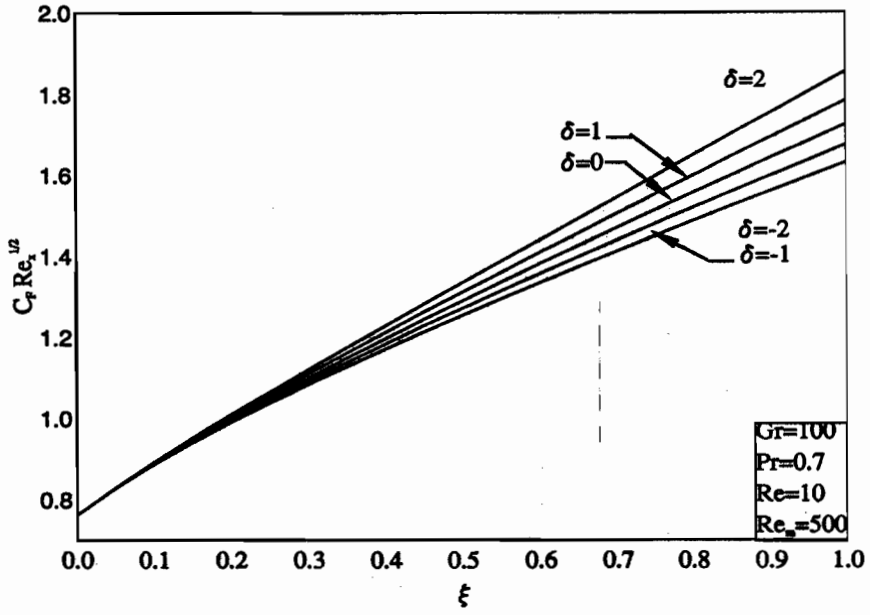

Figure 17. Effect of δ on the local skin-friction coefficient.

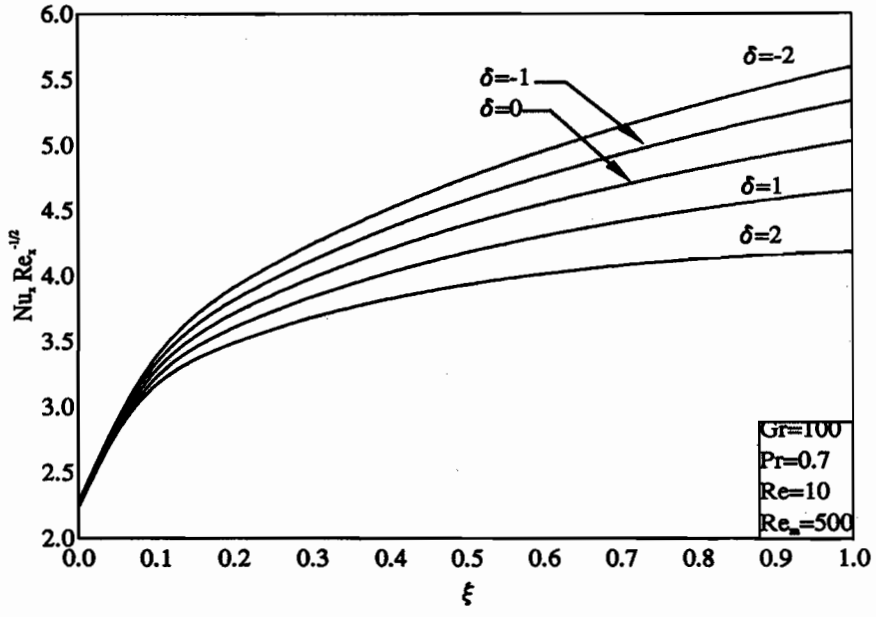

Figure 18. Effect of δ on the local Nusselt number.

Nu_x^* is more sensitive to changes in δ than the skin-friction coefficient C_F^*.

It should be mentioned herein that a similar study for clear fluid flow over a cone and a wedge by Vajravelu and Nayfeh (1992) pointed out that for $\delta > 1$, the flow and heat transfer solutions become oscillatory in nature, indicating instability problems. This behavior can be observed from the simple Darcy model with heat generation for large values of δ. In the present problem with consideration of variable porosity and thermal dispersion effects, it was investigated whether this condition occurs and, if so, for what values of δ. The result of this investigation indicated that for values of δ as high as $\delta = 9$, a very distinctive peak in the temperature profile ($\theta_{max} = 13.13$) occurring at $\eta = 5.95$ was observed. The proper approach to the ambient temperature condition took place at $\eta = 25$. This huge increase in the fluid temperature caused a distinctive maximum in the velocity profile that occurred very close to the plate surface at $\eta = 2.27$, illustrating the channeling effect usually observed in variable porosity studies (see, e.g., Vafai et al., 1985). The approach to the ambient velocity condition occurred at $\eta = 20$. For values of $\delta > 9$ solution convergence problems were encountered, which may be suggesting the instability problems mentioned by Vajravelu and Nayfeh (1992). No results for this situation are reported graphically as $\delta = 9$ may not represent a physical situation.

Figures 19 and 20 present comparisons of the local skin-friction coefficients C_F^* and the local Nusselt number Nu_x^* along the plate for assisting or aiding flow with those corresponding to opposing flow under the same conditions for various values of Gr, respectively. For the case of opposing flow ($Z = -1$) complete solutions in the whole computational domain ($0 \le \xi \le 1$) were not possible. This was due to the flow separation or reversal flow condition near the wall for $\xi > 0.5$. The location of this condition was found to be dependent on the value of Gr or the mixed convection parameter Gr/Re^2. For this reason, C_F^* and Nu_x^* were plotted up to $\xi = 0.5$ in Figs. 19 and 20. It should be mentioned herein that this type of flow reversal phenomenon was previously reported by Kliegel (1959) and Ramachandran et al. (1985). It is observed from Fig. 19 that for vanishing or small values of Gr ($Gr = 0.001$) the skin-friction coefficient C_F^* is constant along the plate for both assisting and opposing flows. However, while C_F^* increases linearly with ξ for assisting flow as Gr increases, it tends to decrease at the same rate for opposing flow. That is, for a specific value of Gr, the distribution of C_F^* along the plate for assisting and opposing flow conditions is symmetric about that corresponding to forced convection ($Gr = 0$). On the other hand, a different behavior is predicted for the wall heat flux along the plate. That is, the local Nusselt number is more sensitive to changes in

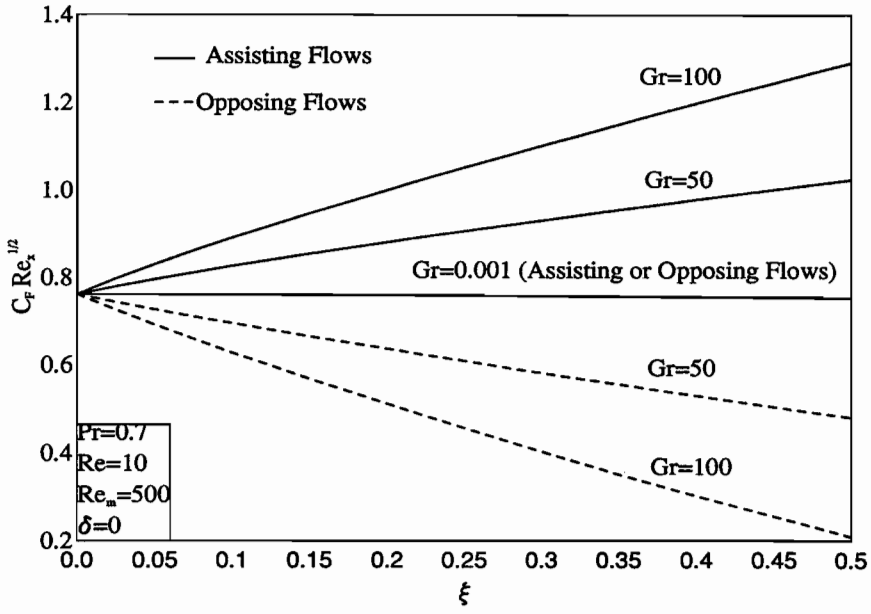

Figure 19. Comparison of the local skin-friction coefficient between assisting and opposing flows.

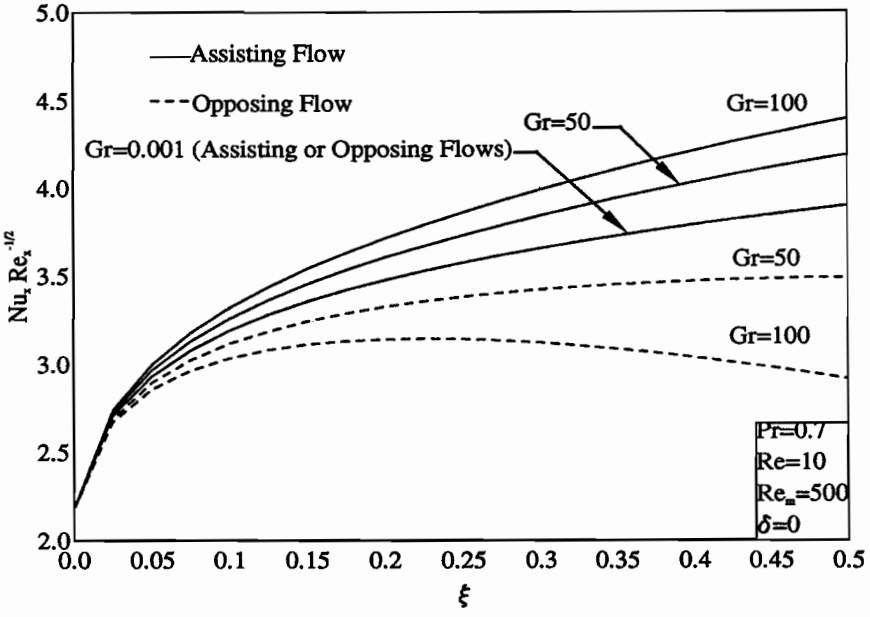

Figure 20. Comparison of the local Nusselt number between assisting and opposing flows.

Gr for opposing flows than for aiding flows. Also, it is observed from Fig. 20 that higher values of Nu_x^* are obtained for aiding flows than those corresponding to opposing flows. In addition, while Nu_x^* increases continuously with ξ for assisting flow, it tends to initially increase and then decrease gradually along the plate for opposing flow at high *Gr* values.

Finally, the physical consequence of including the variable porosity and thermal dispersion effects in the mathematical model on the local Nusselt number Nu_x^* is shown in Fig. 21 for the flow aiding condition. First, the local Nusselt number along the plate in the absence of the porous medium is compared with the numerical and experimental results of Ramachandran et al. (1985) and the experimental data of Kliegel (1959) and found to be in good agreement. In addition, it is predicted that the Nusselt number is constant along the plate if the porosity of the medium is assumed constant and without including the thermal dispersion effects. However, if the porosity is allowed to vary exponentially as discussed earlier, and maintaining the absence of the thermal dispersion effects from the model, a different behavior is predicted in which Nu_x increases with the distance along the plate. Furthermore, when the thermal dispersion effects were included in the model with the porosity kept constant, much higher values of Nu_x^* (almost one order of magnitude higher) than those corresponding to the case without thermal dispersion were predicted for the parametric conditions shown on the figure. For this situation, the Nusselt number is also constant along the plate except in the immediate vicinity of the wall ($\xi < 0.1$). Moreover, when all of the effects (variable porosity and thermal dispersion) were included in the model, the same increasing trend of Nu_x^* with ξ as the corresponding case without dispersion is predicted but the values of Nu_x^* are almost one order of magnitude higher for this case. This figure highlights the importance of both variable porosity and thermal dispersion effects on the Nusselt number and suggests that numerical results based on a model excluding these effects may be misleading.

CONCLUSION

This work focussed on the numerical modeling of steady, laminar combined convection heat transfer from a vertical impermeable semiinfinite isothermal vertical surface embedded in a porous medium having a variable porosity distribution and in the presence of fluid heat generation effects. The porous medium was made up of spherical solid particles and the fluid was assumed to be Newtonian. The governing equations which included the porous medium boundary, inertia, variable porosity, and thermal dispersion effects were transformed into nonsimilar equations and

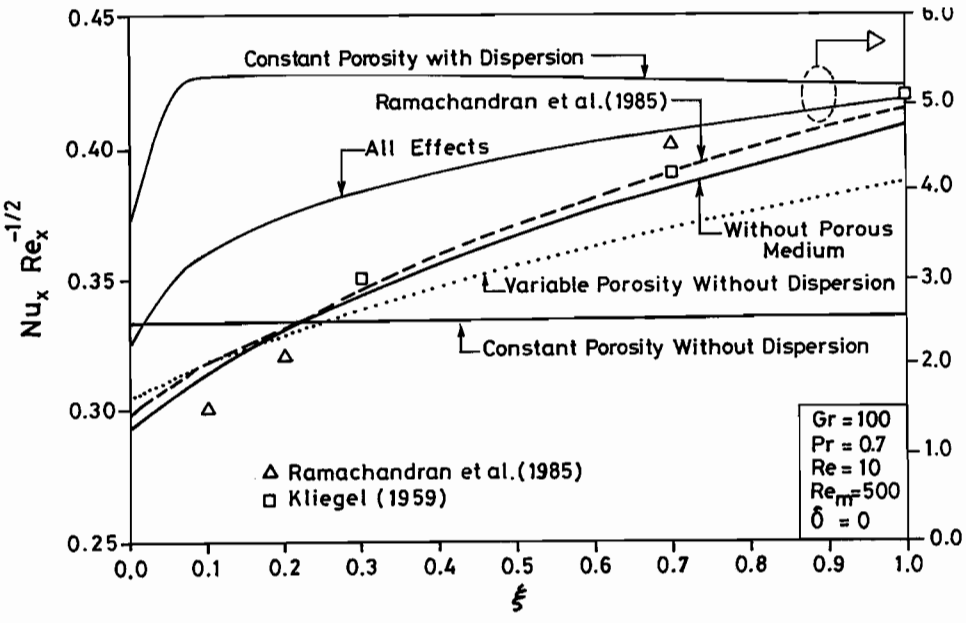

Figure 21. Influence of variable porosity and thermal dispersion on the local Nusselt number.

then solved numerically by an implicit, iterative finite-difference scheme. The accuracy of the numerical method was validated by comparisons with previously published numerical and experimental work on the same problem excluding the porous medium and heat generation effects. A comprehensive parametric study concluded that a reversed flow or a flow separation condition was predicted for the case of opposing flow situation whether the porous medium is present or not. Also, it was found that the local Nusselt number was affected significantly by the inclusion of variable porosity or thermal dispersion effects. This study showed a comparison of the predictive capabilities of various porous media models currently employed by many investigators. Thermal dispersion was found to be the most influential effect among all others. It is hoped that the numerical results reported in this study will serve as a vehicle for understanding the various aspects of porous media modeling and will serve as a stimulus for experimental work on this problem.

REFERENCES

Aldoss, T. K., Al-Nimr, M. A., Jarrah, M. A., and Al-Sha'er, B. J., Magnetohydrodynamic mixed convection from a vertical plate embedded in a porous medium, *Numer. Heat Transfer, Pt A: Appl.*, vol. 28, pp. 635–645, 1995.

Amiri, A. and Vafai, K., Analysis of dispersion effects and non-thermal equilibrium, non-Darcian, variable porosity incompressible flow through porous media, *Int. J. Heat Mass Transfer*, vol. 37, pp. 936–954, 1994.

Benenati, R. F. and Brosilow, C. B., Void fraction distribution in packed beds, *AIChE J.*, vol. 8, pp. 359–361, 1962.

Blottner, F. G., Finite-difference methods of solution of the boundary-layer equations, *AIAA J.*, vol. 8, pp. 193–205, 1970.

Chamkha, A. J., Non-Darcy hydromagnetic free convection from a cone and a wedge in porous media, *Int. Commun. Heat Mass Transfer*, vol. 23, pp. 875–887, 1996.

Chamkha, A. J., Non-Darcy fully developed mixed convection in a porous medium channel with heat generation/absorption and hydromagnetic effects, *J. Numer. Heat Transfer*, Pt A, 1997.

Chen, C.-K. and Chen, C.-H., Nonuniform porosity and non-Darcian effects on conjugate mixed convection heat transfer from a plate fin in porous media, *Int. J. Heat Fluid Flow*, vol. 11, pp. 65–71, 1990.

Cheng, P. and Vortmeyer, D., Transverse thermal dispersion and wall channeling in a packed bed with forced convective flow, *Chem. Engng. Sci.*, vol. 43, pp. 2523–2532, 1988.

Gill, U. S. and Minkowycz, W. J. Boundary and inertia effects on conjugate mixed convection heat transfer from a vertical plate fin in a high-porosity porous medium, *Int. J. Heat Mass Transfer*, vol. 31, pp. 419–427, 1988.

Hishida, K., Yoshida, A., and Maeda, M., Buoyancy effects on boundary layer flow and forced convective heat transfer

over a vertical isothermally heated plate, *ASME-JSME Thermal Engineering Joint Conference,* Honolulu, Hawaii, vol. 3, pp. 163–168, 1983.

Hong, J., Yamada, Y., and Tien, C. L., Effects of non-Darcian and nonuniform porosity on vertical-plate natural convection in porous media, *ASME J. Heat Transfer,* vol. 109, pp. 356–362, 1987.

Hooper, W. B., Chen, T. S., and Armaly, B. F., Mixed convection from a vertical plate in porous media with surface injection or suction, *Numer. Heat Transfer,* Pt A: Appl., vol. 25, pp. 317–329, 1994.

Hsieh, J. C., Chen, T. S., and Armaly, B. F., Mixed convection along a nonisothermal vertical flat plate embedded in a porous medium: the entire regime, *Int. J. Heat Mass Transfer,* vol. 36, pp. 1819–1825, 1993.

Hunt, M. L. and Tien, C. L., Non-Darcian convection in cylindrical packed beds, *J. Heat Transfer,* vol. 110, pp. 378–384, 1988.

Kliegel, J. R., Laminar free and forced convection heat transfer from a vertical flat plate, Ph.D. Thesis, University of California, Berkeley, 1959.

Lloyd, J. R. and Sparrow, E. M., Combined forced and free convection flow on vertical surfaces," *Int. J. Heat Mass Transfer,* vol. 13, pp. 434–438, 1970.

Nithiarasu, P., Seetharamu, K. N., and Sundararajan, T., Natural convective heat transfer in a fluid saturated variable porosity medium, *Int. J. Heat Mass Transfer,* vol. 40, pp. 3955–3967, 1997.

Oosthuizen, P. H. and Hart, R., A numerical study of laminar combined convective flow over flat plates, *ASME J. Heat Transfer,* vol. 95, pp. 60–63, 1973.

Ramachandran, N., Armaly, B. F., and Chen, T. S., Measurements and predictions of laminar mixed convection flow adjacent to a vertical surface, *ASME J. Heat Transfer,* vol. 107, pp. 636–641, 1985.

Schertz, W. M. and Bischoff, K. B., Thermal and material transport in non-isothermal packed beds, *AIChE J.,* vol. 15, pp. 597–604, 1969.

Shenoy, A. V., Darcy natural, forced and mixed convection heat transfer from an isothermal vertical flat plate embedded in a porous medium saturated with an elastic fluid of constant viscosity, *Int. J. Engng. Sci.,* vol. 30, pp. 455–467, 1992.

Sparrow, E. M. and Cess, R. D., Temperature dependent heat sources or sinks in a stagnation point flow, *Appl. Sci. Res.,* vol. A10, pp. 185–197, 1961.

Takhar, H. S., Soundalgekar, V. M., and Gupta, A. S., Mixed convection of an incompressible viscous fluid in a porous medium past a hot vertical plate, *Int. J. Non-Lin. Mech.,* vol. 25, pp. 723–728, 1990.

Vafai, K., Convective flow and heat transfer in variable porosity media, *J. Fluid Mech.,* vol. 147, pp. 233–259, 1984.

Vafai, K., Alkire, R. L., and Tien, C. L., An experimental investigation of heat transfer in variable porosity media, *ASME J. Heat Transfer,* vol. 107, pp. 642–647, 1985.

Vajravelu, K. and Hadjinicolaou, A., Convective heat transfer in an electrically conducting fluid at a stretching surface with uniform free stream, *Int. J. Engng. Sci.,* vol. 35, pp. 1237–1244, 1997.

Vajravelu, K. and Nayfeh, J., Hydromagnetic convection at a cone and a wedge, *Int. Commun. Heat Mass Transfer,* vol. 19, pp. 701–710, 1992.

Wilks, G., Combined forced and free convection flow on vertical surfaces, *Int. J. Heat Mass Transfer,* vol. 16, pp. 1958–1964, 1973.